INTER-DIGITAL H-MODE DRIFT-TUBE LINAC DESIGN WITH ALTERNATIVE PHASE FOCUSING FOR MUON LINAC

M. Otani, T. Mibe, M. Yoshida, KEK, Oho, Tsukuba, 305-0801, Japan
K. Hasegawa, Y. Kondo, JAEA, Tokai, Naka, Ibaraki, 319-1195, Japan
N. Hayashizaki, Tokyo Institute of Technology, Tokyo, 152-8550, Japan
Y. Iwashita, Kyoto University, Kyoto, 611-0011, Japan
Y. Iwata, NIRS, Chiba, 263-8555, Japan R. Kitamura, University of Tokyo, Hongo, 113-8654, Japan
N. Saito, J-PARC Center, Tokai, Naka, Ibaraki, 319-1195, Japan

Abstract

We have developed an inter-digital H-mode (IH) drift-tube linac (DTL) design with an alternative phase focusing (APF) scheme for a muon linac, in order to measure the anomalous magnetic moment and electric dipole moment (EDM) of muons at the Japan Proton Accelerator Research Complex (J-PARC). The IH-DTL accelerates muons from $\beta = v/c = 0.08$ to 0.28 at an operational frequency of 324 MHz. The synchronized phase array is optimized with analytical calculation of the beam dynamics to get smaller emittance growth during acceleration. Then an IH-DTL cavity is modeled in the 3D EM simulation. Finally the beam dynamics in the cavity are evaluated numerically. The output beam emittances are calculated as 0.315π and 0.195π mm mrad in the horizontal and vertical directions, respectively, which satisfies the experimental requirement. Additional emittance growth due to an error field caused by fabrication error is evaluated to be less than 10% with eight slug tuners. The design and results are described in this paper.

INTRODUCTION

The low emittance muon beam has been discussed in several scientific fields [1–3]. One of those is the quest for hunting beyond the Standard Model (SM) of elementary particle physics. In the muon anomalous magnetic moment $(g - 2)_\mu$, there is about three standard deviation between the SM prediction and the measured value with a precision of 0.54 ppm [4]. This discrepancy is thought to be due to interactions or particles that are unknown to the SM; therefore, further investigations are desired. The low emittance muon beam will provide more precise measurement since the dominant systematic uncertainties in the previous experiment resulted from the muon beam dynamics in the muon storage ring.

We are developing a muon linac for the $(g - 2)_\mu$ experiment [5] at Japan Proton Accelerator Research Complex (J-PARC) to realize the low emittance muon beam. Figure 1 shows the muon linac configuration. In order to satisfy the experimental requirement of an extremely small transverse divergence angle of 10^{-5}, the muon should be accelerated to a momentum of 300 MeV/c (212 MeV), without substantial emittance growth. In addition, the effective accelerating gradient should be relatively high, especially in the low β

region (less than 0.28), in order to avoid muon decay loss due to the muon finite lifetime of 2.2 μs. Moreover, the construction cost is desirable to be reduced. Based on these considerations, an IH-DTL incorporating the APF method is employed for the acceleration stage from $\beta = 0.08$ to 0.28.

This paper focuses on the IH-DTL [6] and details of other structures and preparation status can be found in elsewhere [7–9]. In following sections, the APF IH-DTL design and results are described. After that, an error field study is presented.

APF IH-DTL DESIGN

In the APF scheme, the gap-to-gap synchronous phases are varied in order to achieve longitudinal and transverse focusing. However, the synchronous phase array determines each cell length and changes the average on-axis field E_0 at each gap, which in turn affects the particle motion. Hence, the phase array optimization is strongly correlated to the beam dynamics and the cavity design. In order to solve this convoluted problem, the procedure is divided into the following three steps:

A) Synchronous phase array optimization

B) Cavity optimization

C) Particle tracking

In first step, the particle dynamics are calculated analytically using certain approximations and for a particular synchronous phase array. These calculations are performed using "LINACSapf" [10], with some modifications for the dynamics calculations and the synchronized phase array definition to accommodate the π–mode acceleration, whereas 2π–mode acceleration is assumed in the original code. In "LINACSapf", the beam dynamics is calculated by so called *drift-kick-drift method* [11]. One notable difference to softwares for an ion-linac design such as PARMILA [12] is the implementation of the transverse focus and de-focusing due to the radial displacement and the electro-static effect; because velocity evolution in muon acceleration is larger, those effect has about 30% of RF de-focusing only. E_0 is determined from the Kilpatrick criterion [13,14]. The Kilpatrick limit E_{kilpat} at 324 MHz is 17.8 MV/m and a value of approximately $1.8 \times E_{kilpat}$ is employed for the maximum surface field, based on the empirical value applying to RFQs.
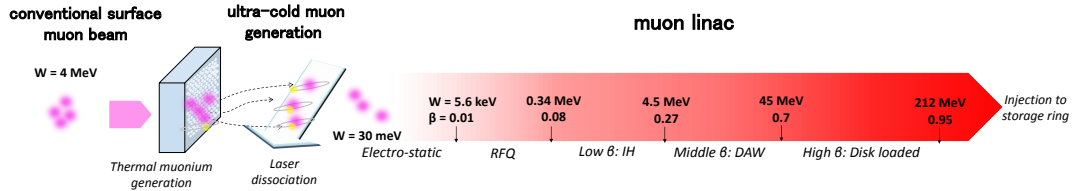
Figure 1: Configuration of low-emittance muon beam.

Assuming that the peak-to-average ratio is three, E_0 is set to 10 MV/m. The maximum surface field will be confirmed following discussion of the cavity design.

In the code, the dimensions of the drift tubes and gaps are calculated with assigned E_0, the particle velocity of the central orbit, and assigned synchronous phase array $\{\phi_n\}$. Then the dynamics of all the particles are calculated. The initial settings of the synchronized phase array are assigned based on those for the HIMAC accelerator [15]. All the $\{\phi_n\}$ are optimized using the minimization function f, which is defined based on the emittance growth ($\Delta\varepsilon$), the energy spread of the output beam (ΔE), and the loss particle efficiency ($\varepsilon_{\mathrm{loss}}$), such that $f = \Delta\varepsilon + \Delta E + \varepsilon_{\mathrm{loss}}$.

Table 1 shows details of the optimized parameters. Gap numbers 1–2, 6–9, 15 and 16 have negative synchronous phases, during which time the beam is longitudinally focused. However, gap numbers 3–5 and 10–14 have positive, during which time the beam is transversely focused. Because the electrostatic focusing is stronger in the lower-beta part, the first collection of positive phase groups has a smaller number of gaps. The output energy is 4.5 MeV with total length of 1.3 m.

the electro-magnetic field and the resonant frequency depend on the entire structure of the IH cavity, and the detail of the overall structure (including the ridges, etc.) should be incorporated in the calculation model. Therefore, the entire IH cavity is modeled using the CST Micro Wave (MW) Studio [16] three-dimensional field solver, in order to calculate the electro-magnetic field. Figure 2 shows the three-dimensional model of the IH cavity in CST MW Studio.
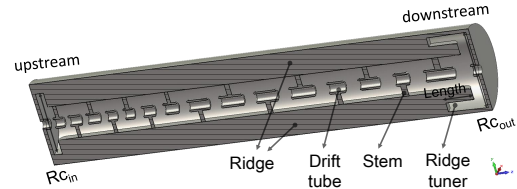

Figure 2: Three-dimensional model of IH cavity in CST MW Studio calculation.

To optimize the IH cavity, the drift tubes and the acceleration gaps are first arranged according to the previously determined optimized parameters shown in Table 1. Because the drift tube and gap length depend on both the synchronous phase and beta, the inductance and capacitance along the cavity are not constant, which distorts the acceleration field. In order to achieve flat electric field on the beam axis E_z, the following dimensions are adjusted: the cavity radius, the ridge tuner length, the cavity taper, the stem radius, and the tube radius.

Note that adjustment of the cavity radius is used to tune the resonant frequency, and the radius tuning does not strongly influence the E_z flatness. The flatness is first optimized through tuning of the other parameters; the resonant frequency is then adjusted by changing the cavity radius.

The E_z flatness is primarily tuned using the ridge tuner and the cavity taper. The black and blue lines in Fig. 3 show the longitudinal electric field along the beam axis before and after these optimizations. Before the optimizations, the field in the downstream region is lower than that in the upstream region, because the acceleration gaps in the downstream region are smaller than those upstream, and the equivalent capacitance gradient results in a field gradient. The tilting field is prescribed by adjusting the ridge tuner length and the cavity taper.

Table 1: Cell Parameters for Optimized Phase Array

cell	W [MeV]	β	ϕ [degrees]	cell length [mm]	total [mm]
1	0.34	0.08	-35.9	29.5	29.5
2	0.43	0.09	-14.9	46.0	75.4
3	0.57	0.10	12.9	54.9	130
4	0.74	0.12	32.9	60.3	191
5	0.92	0.13	15.4	54.4	245
6	1.14	0.15	-13.8	56.0	301
7	1.38	0.16	-31.4	66.4	367
8	1.63	0.17	-44.3	74.1	442
9	1.86	0.19	-18.8	97.2	539
10	2.16	0.20	12.5	108	646
11	2.49	0.21	27.6	106	753
12	2.82	0.23	47.6	116	868
13	3.10	0.24	23.2	94.2	963
14	3.50	0.25	10.8	108	1070
15	3.95	0.27	-34.6	91.5	1160
16	4.30	0.28	-15.6	142	1300
exit	4.50				

As a second step, the IH cavity is modeled in a three-dimensional EM simulation. Because the IH cavity is not axially symmetric, a three-dimensional model is necessary in order to evaluate the electro-magnetic field. In addition,

Fine tuning of E_z in each gap is achieved by changing the stem radius and the drift tube radius, as shown by the red line in Fig. 3. By first adjusting the radius and then varying the equivalent inductive load at each gap, the field differences between the gaps can be corrected. Because the stem radius and the drift tube radius are correlated with the feasibility of the manufacturing process, the range of adjustment is feasible in terms of manufacturing.
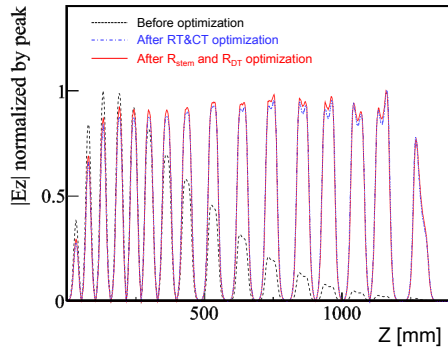

Figure 3: Effects of ridge tuner (RT), cavity taper (CT), stem radius (R_{stem}), and drift tube radius (R_{DT}) adjustment. Horizontal axis is the distance from the cavity start on the beam axis, and vertical axis is the E_z normalized at the peak value. Black: longitudinal electric field along z before optimizations, blue: field after optimizations with RT and CT, red: field after optimizations with R_{stem} and R_{DT}.

The variation in the electric field in the gaps after the optimization is approximately 10%, excluding the first and last cells. The resonant frequency is tuned to a slightly lower value than the 324-MHz operation frequency, in order to leave room for the tuner knobs with the inductive tuner installed on the cavity side wall. The quality factor (Q_0) is calculated to be 1.07×10^4. The effective shunt impedance is calculated to be 92 MΩ/m, and the operation power power is required to be 250 kW. The effective shunt impedance is competitive to those of other IH structures given our IH application to relatively higher velocity region.

The maximum surface field is evaluated to be 34 MV/m at the outer surface of the most downstream drift tube, corresponding to 1.9 times the Kilpatrick limit. This value is reasonable based on the experiences in RFQs.

In third step, the beam particle trajectory is simulated using the General Particle Tracer (GPT) [17]. In GPT, the dynamics is calculated with an embedded fifth order Runge-Kutta driver with the sufficiently small step size. The electric and magnetic fields calculated using CST MW Studio are implemented in the code and the particle dynamics are calculated numerically. The number of simulated particles is 10^5 that corresponds to designed muon beam intensity per bunch.

Figure 4 (top) shows the normalized velocity in the x-direction along the beam axis (z) with overwriting of the synchronous phase (ϕ). As shown in the red hatched box in Fig. 4, the synchronous phases are positive for z = 130–

250 mm and 650–1070 mm, where the transverse focusing is implemented. During these periods, the horizontal velocity is decreased.

Figure 4 (bottom) shows the normalized velocity in the y-direction along the beam axis. The vertical trajectory is dominated by the finite value of the vertical electric field. In order to reduce the additional growth, some conventional solutions, such as the use of drift tube bulges [18], have been considered. However, this approach only reduces the vertical field of the IH structure with few percents because the cell length is relatively large (because of the application of the IH structure to yield a higher β region). As a result, no sufficient suppression of the extra growth is achieved using these the additional structures. Because the extra growth is acceptably small and the output beam satisfies the requirement of the J-PARC $(g - 2)_\mu$ experiment , no additional structures are implemented in this design, so as to avoid additional power loss at these structures.
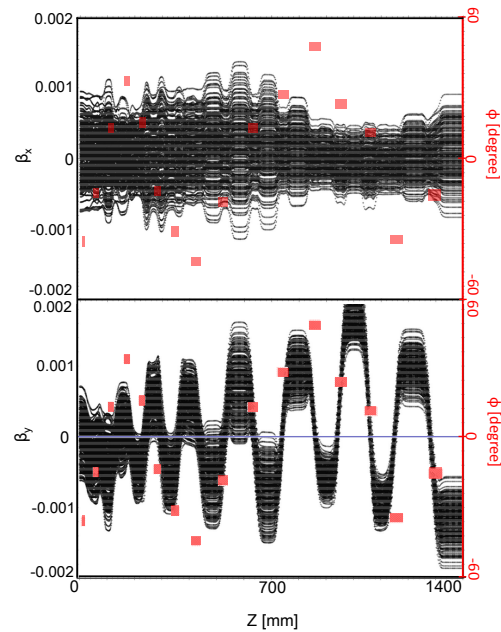

Figure 4: Beam velocity distribution as a function of distance along the IH structure (black) and synchronous phase in each position (red). β_x (top) and β_y (bottom) along beam axis.

Finally, the output beam is evaluated using realistic input beam distributions. The input beam was obtained from simulations of the surface muon beamline, the ultra slow muon system, and the RFQ [19]. From the results, the normalized root mean square (rms) emittances of the input beam were evaluated as 0.297π mm mrad in the x-direction, 0.168π mm mrad in the y-direction, and 0.0181π MeV deg in the z-direction. Because the structure is not periodic due to the APF method and rapidly changing velocity profile, the twiss parameters (α and β) at the IH entrance were scanned in order to obtain a matching condition to the IH,

instead of the conventional method solving a periodic solution of the transfer matrix. Based on the scan results, the transport line from the RFQ to the IH was designed using TRACE3D [20], and the beam distributions at the RFQ exit were then transported using PARMILA [12]. Figure 5 shows the calculated phase-space distributions of the output beam. The emittance growth was calculated to be 0.018π (6.1%) and 0.027π mm mrad (16%) in the x- and y-directions, respectively. This is consistent with the evaluations using the wb distribution to within a few percent, and the small discrepancy is due to the difference in the distribution shape in the z-direction. The transmission efficiency without any selections in output beam was calculated to be 99.9%. The beam transit time $t_{\text{tran.}}$ was 25 ns and the muon survival rate is calculated to be $\exp(t_{\text{tran.}}/\tau_\mu \overline{\gamma}) = 98.9\%$, where the average Lorentz factor during acceleration is labeled $\overline{\gamma}$. The total transmission is expected to be 98.7%, which is sufficient for the J-PARC $(g-2)_\mu$ experiment.
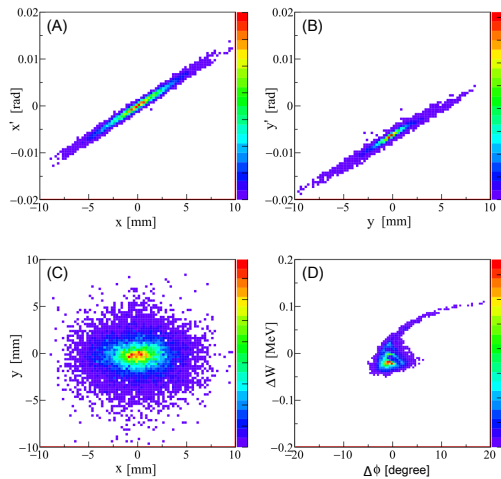

Figure 5: Calculated phase space distributions at IH exit. (A) the horizontal divergence angle x' vs x, (B) the vertical divergence angle y' vs y, (C) y vs x, and (D) $\Delta W(W-4.5$ MeV) vs $\Delta\phi$.

In conclusion, the beam emittance will meet the requirement for the J-PARC $g-2$/EDM experiment.

ERROR FIELD STUDY

Since beam stability relies on the RF field in the APF method, the beam dynamics may be strongly affected by an error field. In order to estimate the error field effect to the emittance growth, the RF field in each gap is scaled by a range of few percents independently and then the beam dynamics in the scaled fields are calculated numerically. The emittances of the output beam are calculated with 50 sets of the pseudo RF field and sum of the average shift and rms is evaluated as the additional emittance growth $\Delta\varepsilon$. Figure 6 shows $\Delta\varepsilon$ as a function of the scaled factor. Because fluctuation of the emittance is larger in the y-direction due to the vertical field, $\Delta\varepsilon_y$ is slightly larger than $\Delta\varepsilon_x$. The field

error is required to be less than 2% to suppress additional emittance growth with less than 10%.
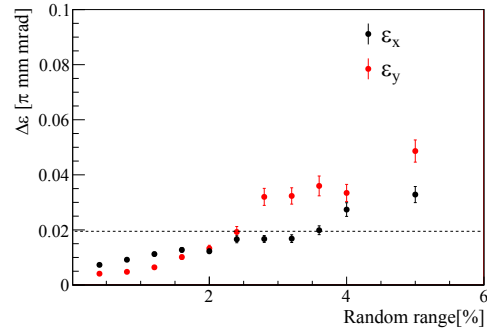

Figure 6: Additional emittance growth as a function of the field scale factor.

One possible cause of an error field is a fabrication error. Because our operational frequency is slightly higher than existing IH-DTL, the fabrication error may be significant impact. In order to estimate the fabrication error effect, some dimensions in the IH model in CST MW Studio are artificially changed and the axial field variations are investigated. Figure 7 shows the field variation when one of the drift tube outer radius is changed. The change is 2% in maximum with general fabrication error of 100 um. Other dimensions such as the drift tube inner radius, stem radius, and incline of the tube and stem are also investigated. It reveals that the field error is about 2% when the fabrication error is less than 100 um.
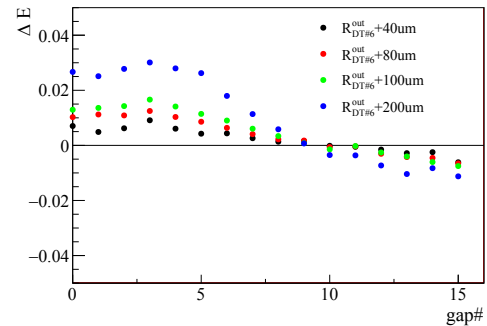

Figure 7: Variation of the axial field peak in each gap when one of the drift tube outer radius is changed.

Since the error field due to the general fabrication error of 100 um is expected to be comparable to the requirements for 10% additional emittance growth, a slug tuner is studied as the field tuner. Figure 10 shows the field variation when the slug tuner is inserted. The error field distribution is consistent with the mode mixing of higher mode of TE111 whose resonant frequency is higher with about 6 MHz than operational mode of TE110. Because there is a clause at $z = 800$ mm in the TE111 resonant field, it is important to set more tuners around that position and mix higher mode of TE112, in order to get higher tuning capability. The

calculation with several setting of the slug tuner shows good linearity of the field variation to the tuner length.
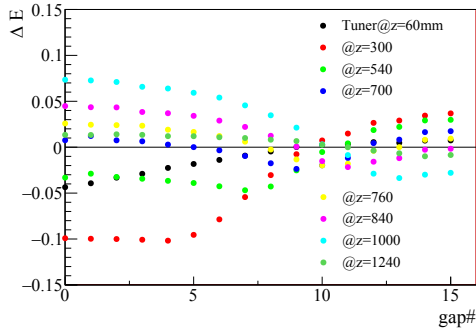

Figure 8: Field variation with the slug tuner at several positions.

Finally we perform a case study assuming the fabrication errors of 100 um. First the electro-magnetic field is calculated with the IH model in which the drift tube inner and outer radii, stem radius and its inclination are independently changed within assigned fabrication error. Assuming the linearity of the length to the field variation, we can write

$$\Delta E_i = \sum_j^{\text{tuners}} \frac{\partial E_i}{\partial L_j} L_j \tag{1}$$

where E_i is the axial field in i'th gap, L_j is the j'th tuner length, and $\frac{\partial E_i}{\partial L_j}$ is the response matrix for the j'th tuner which was estimated by CST MW Studio. The set of L_j is optimized to correct the error field and the electro-magnetic field is calculated again with the tuners. Figure 9 shows one of the results. The difference between design and calculated value is less than 2% with the tuners whereas it is 6% without tuners. The case studies are performed five times and the difference to the design value is almost within 2% with the tuners, as shown in Fig. 10.
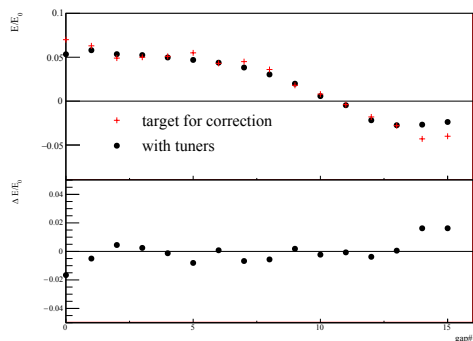

Figure 9: Example of the case study result. Red cross: target value to correct the field error due to the fabrication error, black: actual field with optimized slug tuner length.

In conclusion, the tuning capability against nominal fabrication error with the slug tuners is enough.
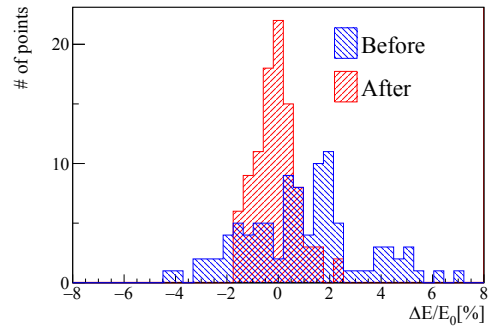

Figure 10: Difference to the design value of the electric field on each gap. Blue: difference without the tuners, red: difference with the tuners.

REFERENCES

[1] M. Palmer *et al.*, ICFA Beam Dynamics Newsletter, No.55, 2011; http://icfa-usa.jlab.org/archive/newsletter/icfa_bd_nl_55.pdf

[2] Y. Miyake *et al.*, Hyperfine Interact, 216, p.79, 2013.

[3] M. Bogomilov *et al.*, JINST 7, P05009, 2012.

[4] G.W. Bennett *et al.*, Phys. Rev. D73, 072003, 2006.

[5] J-PARC E34 conceptual design report, 2011. (unpublished); https://kds.kek.jp/indico/event/8711/material/2/0.pdf

[6] M. Otani *et al.*, Phys. Rev. Accel. Beams, 19, 040101, 2016.

[7] M. Otani *et al.*, Proc. of IPAC2016, TUPMY003.

[8] Y. Kondo *et al.*, PASJ2016 Proc., MOOM04.

[9] R. Kitamura *et al.*, PASJ2016 Proc., MOP050.

[10] R.A. Jameson, arXiv:1404.5176 [physics.acc-ph].

[11] T.P. Wangler, "RF Linear Accelerators", WILEY-VCH Verlag, GmbH&Co, 2011.

[12] Los Alamos Accelerator Code Group (LAACG), LANL, Los Alamos; http://www.laacg.lanl.gov

[13] W.D. Kilpatrick, Rev. Sci. Instr. 28, 824, 1957.

[14] T.J. Boyd Jr., Los Alamos Group AT-1 report AT-1:82-28, 1982.

[15] Y. Iwata *et al.*, Nucl. Instr. Meth. A569, 685, 2006.

[16] CST Studio Suite, Computer Simulation Technology (CST); https://www.cst.com/products/CSTMWS

[17] GPT, Pulsar Physics; http://www.pulsar.nl/gpt/

[18] S.S. Kurennoy *et al.*, Phys. Rev. ST Accel. Beams 15, 090101, 2012.

[19] Y. Kondo *et al.*, Proc. of IPAC2015, 2015, THPF045, 2015.

[20] K.R. Crandall and D.P. Rustoi, Los Alamos Report, No. LA-UR-97-886, 1997.